Ann. Geophys., 27, 1625–1629, 2009
www.ann-geophys.net/27/1625/2009/

Annales Geophysicae

Characteristics of equatorial gravity waves derived from mesospheric airglow imaging observations

S. Suzuki[1], K. Shiokawa[2], A. Z. Liu[3], Y. Otsuka[2], T. Ogawa[2,*], and T. Nakamura[4]

[1]Sugadaira Space Radio Observatory, University of Electro-Communications, Chofu, Tokyo, Japan
[2]Solar-Terrestrial Environment Laboratory, Nagoya University, Nagoya, Aichi, Japan
[3]Department of Electrical and Computer Engineering, University of Illinois at Urbana-Champaign, Urbana, IL, USA
[4]Research Institute for Sustainable Humanosphere, Kyoto University, Uji, Kyoto, Japan
[*]now at: National Institute of Information and Communications Technology, Koganei, Tokyo, Japan

Received: 30 January 2009 – Accepted: 11 March 2009 – Published: 6 April 2009

Abstract. We present the characteristics of small-scale (<100 km) gravity waves in the equatorial mesopause region derived from OH airglow imaging observations at Kototabang (100.3° E, 0.2° S), Indonesia, from 2002 to 2005. We adopted a method that could automatically detect gravity waves in the airglow images using two-dimensional cross power spectra of gravity waves. The propagation directions of the waves were likely controlled by zonal filtering due to stratospheric mean winds that show a quasi-biennial oscillation (QBO) and the presence of many wave sources in the troposphere.

Keywords. Atmospheric composition and structure (Airglow and aurora) – Meteorology and atmospheric dynamics (Thermospheric dynamics; Waves and tides)

1 Introduction

Gravity waves control the wind/thermal balance in the mesosphere and lower thermosphere (MLT) through wave dissipation and the accompanying momentum flux divergence Fritts and Alexander (2003). Airglow imaging observations reveal two-dimensional (2-D) characteristics of small-scale (less than ∼100 km) gravity waves in the upper mesosphere (e.g., Taylor et al., 1995). On the basis of long-term imaging observations at several locations, it has been observed that the wave characteristics have seasonal/geographical dependence (Suzuki et al., 2009, and references therein). In particular, the horizontal propagation directions of gravity waves show the dependence clearly because the propagation direction is greatly influenced by the background atmospheric conditions in the propagation paths and by the locations of the wave sources.

Recently, several attempts have been made to identify gravity wave structures in airglow images by using the auto-detection method. This method provides unbiased dataset of gravity waves as opposed to the method involving visual inspections, and also helps in the quantitative estimation of the momentum flux. Tang et al. (2005a) introduced a novel computational technique to identify gravity wave components by using 2-D cross power spectra of all-sky OH airglow images. This technique also provides the gravity wave momentum flux when the model of Swenson and Liu (1998) is used; this model relates the momentum flux to the wave parameters that can be derived from airglow images (Tang et al., 2005a,b; Suzuki et al., 2007).

In this paper, we present a statistical study on the gravity waves derived by the auto-detection method from OH airglow images obtained at an equatorial observatory (0.2° S). On the basis of the statistics, we show for the first time that quasi-biennial oscillation (QBO) is an important factor to control horizontal propagation direction of the equatorial gravity waves.

2 Instrumentations and observations

In this study, we used an all-sky imager that was installed as part of the optical mesosphere thermosphere imagers (OMTIs, Shiokawa et al., 2009) at Kototabang (100.3° E, 0.2° S), Indonesia, in October 2002. OH airglow (720–910 nm) images are taken every 4.5 min with a 15-s exposure.

For the present study, we used the OH airglow images collected between October 2002 and June 2005. Our analysis concentrates on clear-sky nights (i.e., on the nights when

Correspondence to: S. Suzuki
(shin.s@ice.uec.ac.jp)

Published by Copernicus Publications on behalf of the European Geosciences Union.

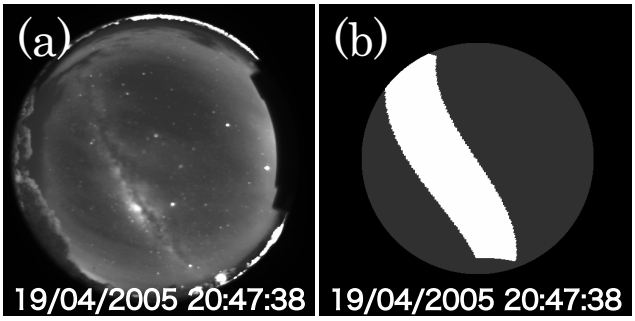

Fig. 1. (a) Example of an all-sky OH airglow image obtained at Kototabang on 19 April 2005 (20:47 UT). **(b)** All-sky Milky Way area modeled for the same time.

there were no clouds for at least 1 h) with simultaneous meteor wind measurements at Kototabang to obtain the intrinsic wave parameters. Because of the tropical cloudy weather at Kototabang, the available data are limited to 26 nights.

3 Method of analysis

We adopted the automated method described by Suzuki et al. (2007) to identify gravity wave structures and calculate their momentum fluxes from the all-sky images. This method is based on the scheme developed by Tang et al. (2005a) and provides wave parameters (horizontal wavenumber k, phase speed c, and wave amplitude in the airglow intensity I'/I, where I' is perturbation of intensity I) from every set of images; each set of images contains three consecutive airglow images, i.e., every 13.5 min (=4.5-min×3). In this paper, we define a "wave event" as the wave identified in a set.

We now briefly describe the procedures of this study. First, optical contaminations in the airglow images, such as stars and background continuum emissions, are attenuated. Then the all-sky images are projected onto the geographical coordinates with a size of $512\times512\,km^2$ by assuming an emission height of 86 km.

Second, contaminations from large-scale structures, such as inhomogeneity due to the imager optics, are removed from the images by subtracting the median over a size of $100\times100\,km^2$ from each pixel count. Then the time difference (TD) between two sequential images is obtained. However, the contaminations caused by the Milky Way in the images obtained at Kototabang are often extremely high and are clearly evident in the TD images. Therefore, it is necessary to perform the following processes before the geographical projection: (i) An averaged sky map is prepared in the equatorial coordinates (declination, right ascension) by averaging the airglow images observed on clear-sky nights to define the Milky Way area. (ii) An all-sky Milky Way area is created from the averaged sky map for the acquisition time of each airglow image. Figure 1 shows an all-sky airglow image (raw image) and an all-sky Milky Way area on 19 April 2005, at 20:47 UT. The Milky Way area sufficiently covers the Milky Way structure in the airglow image. (iii) Both the all-sky airglow and Milky Way images are projected onto the geographical coordinates. (iv) After the detrending process, when the pixel count in the detrended image within the Milky Way area are larger than the mean of the whole image, the pixel count is replaced by the mean.

Finally, gravity waves with an intensity amplitude greater than 0.5% and horizontal wavelength in the range of 20–100 km are identified from 2-D cross power spectra of the sequential TD images. This procedure can distinguish several waves with different wave parameters with a single set of images; this is because every wave appears as an individual peak in the 2-D power spectra.

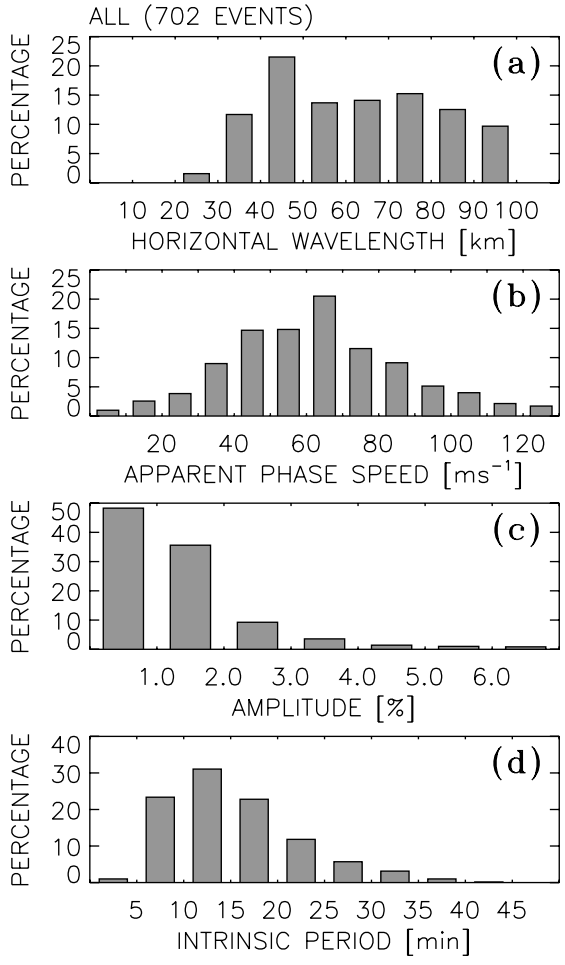

Fig. 2. Histograms of gravity wave parameters in OH airglow images. **(a)** Horizontal wavelength, **(b)** apparent horizontal phase speed, **(c)** amplitude in airglow intensity, and **(d)** intrinsic wave period.

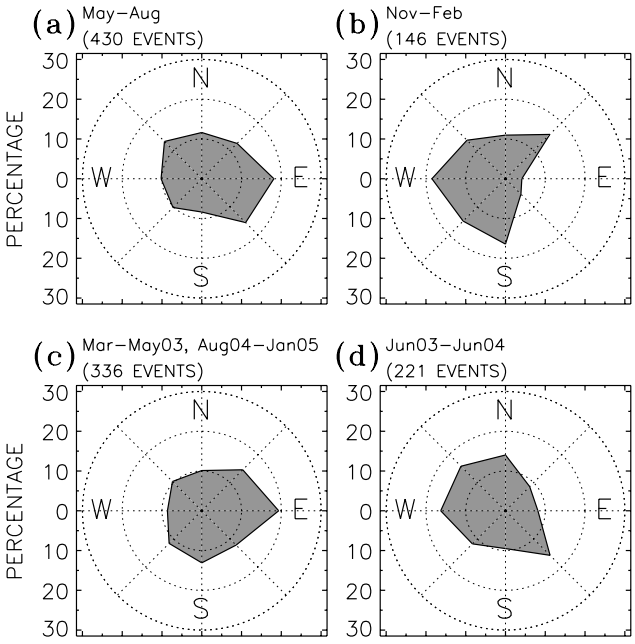

Fig. 3. Seasonal variations in the horizontal propagation directions of the gravity waves: **(a)** May–August and **(b)** November–February. The scale indicates the fraction (in percent) of gravity waves propagating in each direction. The bottom panels show the horizontal propagation directions during **(c)** March–May 2003 and August 2004 to January 2005 and **(d)** June 2003 to June 2004, coinciding with the westward and eastward phases of the QBO, respectively.

4 Statistical results

Figure 2 shows the histograms of the gravity wave parameters derived from the OH images obtained at Kototabang (total: 702 events). The horizontal wavelength $\lambda_h(=2\pi/k)$ (panel a) and the phase speed (panel b) showed peaks in the range of 40–50 km and 60–70 ms^{-1}, respectively. The airglow intensity amplitude (panel c) and intrinsic wave period $\tau(=\lambda_h/|c-u|$, where u is the wind at 86 km in the direction of wave propagation provided from the collocated meteor radar) (panel d) were mostly less than 3% and between 5 and 25 min, respectively. Similar distributions of wave parameters were reported in the previous observations at other sites (Suzuki et al., 2009, and references therein). The phase speeds obtained in the present study were slightly greater than those at midlatitudes. Similar gravity waves with large phase speeds ($\sim$70 ms^{-1}) were reported in the statistics at equatorial latitudes (e.g., Nakamura et al., 2003; Wrasse et al., 2006).

According to recent observations, the horizontal propagation direction of gravity waves shows a clear seasonal dependence, in agreement with the background atmospheric conditions (e.g., Shiokawa et al., 2009). We now divide the 12 months of a year into four seasons: March–April, May–August, September–October, and November–February, considering two major types of atmospheric conditions (summer and winter). Figure 3a and b shows the propagation directions in winter and summer, respectively, in the Southern Hemisphere. The waves can propagate in all directions. However, slight preferences in the zonal directions are seen in both seasons: 46% (vs. 36%) of the waves propagated eastward (westward) during May–August, while 47% (vs. 25%) of the waves propagated westward (eastward) during November–February. No such a seasonal dependence was observed in the case of the other parameters.

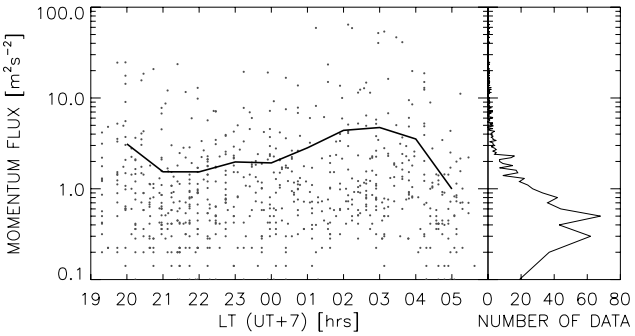

Fig. 4. Variations in the momentum flux magnitudes (log scale) with local time and distributions of the magnitudes. The solid curve in the left panel indicates the hourly mean.

Figure 4 shows the scatter plots of the magnitudes of the momentum flux F_m against the local time variations (left) and distribution of the magnitudes (right). F_m is given by

$$F_m = \frac{1}{2}\frac{m}{k}\frac{\hat{\omega}^2 g^2}{N^4 C_F^2}\left(\frac{I'}{I}\right)^2, \quad (1)$$

where $\hat{\omega}(=2\pi/\tau)$ is the intrinsic frequency, g is the gravitational acceleration, N is the Brunt-Väisälä frequency (typically $\sim$0.02 rad s^{-1}), and C_F is the cancellation factor introduced by Swenson and Liu (1998). The vertical wavenumber m is calculated by using the linear dispersion relation $m{=}k^2(N^2{-}\hat{\omega}^2)/\hat{\omega}^2$. To avoid the uncertainty in the estimated F_m values, the vertical wavelength $\lambda_z(=2\pi/m)$ is fixed in the range of 12–60 km (Suzuki et al., 2007). Although the magnitudes of F_m are scattered widely in the range of 0.1–100 $\mathrm{m}^2\,\mathrm{s}^{-2}$, the dominant is less than 10 $\mathrm{m}^2\,\mathrm{s}^{-2}$ (more than 90% of the total wave events). The hourly means indicated by the solid curve in the left panel do not vary significantly with local time. Mean and standard deviation of F_m were 2.6 $\mathrm{m}^2\,\mathrm{s}^{-2}$ and 6.3 $\mathrm{m}^2\,\mathrm{s}^{-2}$, respectively. This value is roughly comparable to previous estimates of F_m from airglow images (Tang et al., 2005a,b; Espy et al., 2004). These estimates are also comparable to the momentum fluxes obtained from atmospheric radars ($\sim$1–10 $\mathrm{m}^2\,\mathrm{s}^{-2}$, see the review of Fritts and Alexander, 2003), although radar techniques measure gravity waves with larger spatial scales.

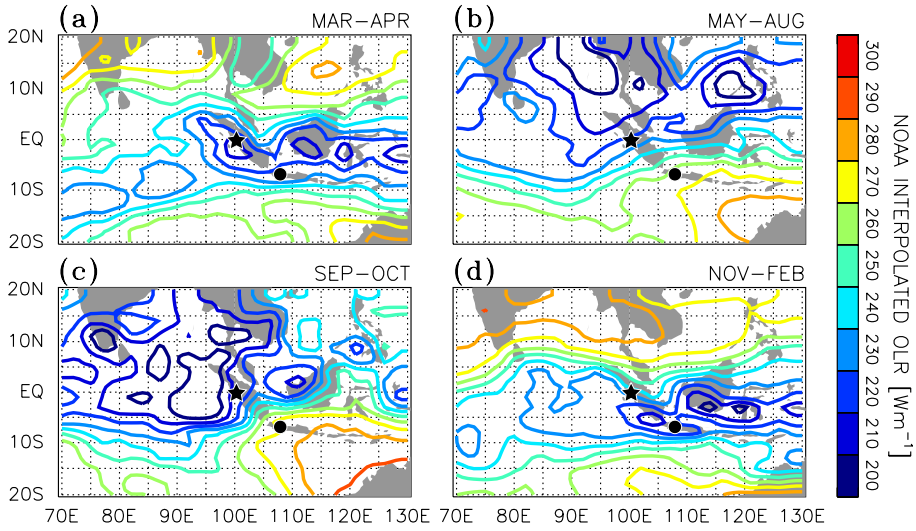

Fig. 5. Averaged OLR map over West-Indonesia for **(a)** March–April, **(b)** May–August, **(c)** September–October, and **(d)** November–February. The black star and circle indicate the locations of Kototabang and Tanjungsari, respectively.

Note that F_m estimated above might have been affected by the Milky Way removal procedures, which might cause the underestimation of I'/I, because the airglow images are partially masked. If the pixels in the whole Milky Way area in Fig. 1b were to be masked, I'/I would be estimated to be ∼70% of the actual amplitude. Since F_m is proportional to $(I'/I)^2$, this would have resulted in a maximum underestimation of ∼50% for F_m. However, pixels with serious count enhancement by the Milky Way constitute a very small part of the whole Milky Way area shown in Fig. 1b, and hence, the underestimation in Fig. 4 is probably much smaller than this estimation.

5 Discussions

In this section, we discuss the propagation directions of the observed gravity waves.

Nakamura et al. (1999) reported that the preferred directions of gravity wave propagation at Shigaraki, Japan (136.1° E, 34.8° N) were eastward in summer and westward in winter, suggesting critical-level filtering by the mesospheric zonal winds flowing westward in summer and eastward in winter. However, the mesospheric winds over the equator were significantly weak (HWM-93) and were not likely to filter the gravity waves.

It is known that at the equatorial latitudes, the QBO dominates dynamics of the stratosphere (e.g., Hamilton, 1984). Tsuda et al. (2006) showed a clear quasi-biennial zonal wind oscillation with an amplitude of ∼30 ms^{-1} over the Indonesian maritime continent from January 2001 to December 2004. We investigated the effect of the QBO on the directions of propagation at Kototabang by classifying the long-term data into subgroups of different QBO phases in reference to the results of Tsuda et al. (2006). Figure 3c and d shows the horizontal propagation directions of the observed gravity waves in March–May 2003, August 2004 to January 2005 (both intervals corresponding to the westward phase of the QBO), and June 2003 to June 2004 (eastward phase). It can be seen that the wave propagated preferentially in the opposite directions to the QBO phase: 46% (vs. 31%) of the waves propagated eastward (westward) during the westward QBO phase, while 44% (vs. 33%) of the waves propagated westward (eastward) during the eastward QBO phase. This suggests that the waves propagating along the QBO phase are filtered out by the stratospheric winds. An identical tendency is recognized in the mean zonal momentum flux: $-2.1\pm10\,\mathrm{m^2\,s^{-2}}$ (positive eastward) during the eastward QBO phase and $-0.1\pm6.2\,\mathrm{m^2\,s^{-2}}$ during the westward phase.

The wave propagation directions also depend on the locations of the wave sources. Nakamura et al. (2003) studied the OH airglow images obtained at Tanjungsari, Indonesia (107.9° E, 6.9° S), about 7° south of Kototabang, and reported that gravity waves showed southward propagation throughout the year. Satellite cloud images suggested that the gravity waves propagated southward because of the wave sources to the north of Tanjungsari, where cloud activity was high. However, at Kototabang, such a strong preference was not seen in the observed directionality.

Figure 5 shows the averaged outgoing longwave radiation (OLR) maps over Kototabang and Tanjungsari for the four seasons. A low OLR indicates a large cloud-top altitude, that is, convection could be high over that location. Figure 5 also indicates that highly active convections occur over

Kototabang throughout the year, which is consistent with the high cloud activity near the equator reported by Nakamura et al. (2003). The less preference of propagation direction of waves at Kototabang compared with Tanjungsari was probably caused by the waves generated by convections over Kototabang. In addition, the preferential propagation of the waves eastward (May–August) and westward (November–February) in Fig. 3a and b is also consistent with the locations of the deep-convection areas in Fig. 5: to the west (east) of Kototabang during May–August (November–February).

6 Summary

We have presented statistics of equatorial gravity waves derived from the OH airglow images obtained at Kototabang by using an auto-detection method for identifying the waves. The results can be summarized as follows:

1. The horizontal wavelengths and the apparent phase speeds were mainly distributed in the range of 30–90 km and 40–70 ms^{-1}, respectively.

2. The intensity amplitudes were less than 3% and the intrinsic wave periods were mostly between 5 and 25 min.

3. The gravity waves propagated with slight preference of eastward (May–August) and westward (November–February), although the strong preferential directionality reported in previous studies at the tropics was not recognized. The directionalities of wave propagation were likely to be determined by the locations of the tropospheric sources. Moreover, the critical-level filtering due to the stratospheric QBO may be also an important factor at the equatorial latitudes.

4. The mean momentum flux magnitude was 2.6 $m^2 s^{-2}$. The variations in the momentum fluxes in the zonal directions are consistent with the QBO phases when considering the critical-level filtering.

Acknowledgements. Y. Katoh and M. Satoh are gratefully acknowledged for their skillful support in the airglow measurements. This work was supported by a Grant-in-Aid for Scientific Research (11440145, 13573006, and Priority Area 764) and Dynamics of the Sun-Earth-Life Interactive System (No. G-4, the 21st Century COE Program). This work was conducted during S.S's visit to UIUC; the visit was supported by a JSPS fellowship (17·7673). The interpolated OLR data were provided by NOAA/OAR/ESRL PSD, Boulder, Colorado, USA (http://www.cdc.noaa.gov/).

Topical Editor C. Jacobi thanks one anonymous referee for her/his help in evaluating this paper.

References

Espy, P. J., Jones, G. O. L., Swenson, G. R., Tang, J., and Taylor, M. J.: Seasonal variations of the gravity wave momentum flux in the Antarctic mesosphere and lower thermosphere, J. Geophys. Res., 109, D23109, doi:10.1029/2003JD004446, 2004.

Fritts, D. C. and Alexander, M. J.: Gravity wave dynamics and effects in the middle atmosphere, Rev. Geophys., 41(1), 1003, doi:10.1029/2001RG000106, 2003.

Hamilton, K.: Mean wind evolution through the quasi-biennial cycle in the tropical lower stratosphere, J. Atmos. Sci., 41, 2113–2125, 1984.

Nakamura, T., Higashikawa, A., Tsuda, T., and Matsushita, Y.: Seasonal variations of gravity wave structures in OH airglow with a CCD imager at Shigaraki, Earth Planets Space, 51, 897–906, 1999.

Nakamura, T., Aono, T., Tsuda, T., Admiranto, A. G., Achmad, E., and Suranto: Mesospheric gravity waves over a tropical convective region observed by OH airglow imaging in Indonesia, Geophys. Res. Lett., 30(17), 1882, doi:10.1029/2003GL017619, 2003.

Shiokawa, K., Otsuka, Y., and Ogawa, T.: Propagation characteristics of nighttime mesospheric and thermospheric waves observed by optical mesosphere thermosphere imagers at middle and low latitudes, Earth Planets Space, in press, 2009.

Suzuki, S., Shiokawa, K., Otsuka, Y., Ogawa, T., Kubota, M., Tsutsumi, M., Nakamura, T., and Fritts, D. C.: Gravity wave momentum flux in the upper mesosphere derived from OH airglow imaging measurements, Earth Planets Space, 59, 421–428, 2007.

Suzuki, S., Shiokawa, K., Hosokawa, K., Nakamura, K., and Hocking, W. K.: Statistical characteristics of polar cap mesospheric gravity waves observed by an all-sky airglow imager at Resolute Bay, Canada , J. Geophys. Res., 114, A01311, doi:10.1029/2008JA013652, 2009.

Swenson, G. R. and Liu, A. Z.: A model for calculating acoustic gravity wave energy and momentum flux in the mesosphere from OH airglow, Geophys. Res. Lett., 25, 477–480, 1998.

Tang, J., Kamalabadi, F., Franke, S. J., Liu, A. Z., and Swenson, G. R.: Estimation of gravity wave momentum flux with spectroscopic imaging, IEEE Trans. Geosci. Remote Sens., 43, 103–109, 2005a.

Tang, J., Swenson, G. R., Liu, A. Z., and Kamalabadi, F.: Observational investigations of gravity wave momentum flux with spectroscopic imaging, J. Geophys. Res., 110, D09S09, doi:10.1029/2004JD004778, 2005b.

Taylor, M. J., Bishop, M. B., and Taylor, V.: All-sky measurements of short period waves imaged in the OI (557.7 nm), Na (589.2 nm) and near infrared OH and O_2 (0, 1) nightglow emissions during the ALOHA-93 campaign, Geophys. Res. Lett., 22, 2833–2836, 1995.

Tsuda, T., Ratnam, M. V., Kozu, T., and Mori, S.: Characteristics of 10-day Kelvin wave observed with radiosondes and CHAMP/GPS Occultation during the CPEA campaign (April–May, 2004), J. Meteorol. Soc. Japan, 84A, 277–293, 2006.

Wrasse, C. M., Nakamura, T., Tsuda, T., Takahashi, H., Medeiros, A. F., Taylor, M. J., Gobbi, D., Salatun, A., Suratno, Achmad, E., and Admiranto, A. G.: Reverse ray tracing of the mesospheric gravity waves observed at 23° S (Brazil) and 7° S (Indonesia) in airglow imagers, J. Atmos. Terr. Phys., 68, 163–181, 2006.